Fault Tolerance of Magnetic Bearings with Material Path Reluctances and Fringing Factors

Uhn Joo Na and Alan B. Palazzolo

***Abstract*—An equivalent magnetic circuit of an eight-pole heteropolar magnetic bearing with path reluctances is developed with nondimensional forms of flux, flux density, and magnetic force equations. The results show that fluxes and magnetic forces are considerably reduced for the magnetic circuit with relatively large path reluctances. A Lagrange multiplier optimization method is used to determine current distribution matrices for the magnetic bearing with large path reluctances. A cost function is defined in a manner that represents load capacity in a specific direction. Optimizing this cost function yields distribution matrices calculated for certain combinations of five poles failed out of eight poles. Position stiffnesses and voltage stiffnesses are calculated for the fault-tolerant magnetic bearings. Fault-tolerant control of a horizontal rigid rotor supported on multiple-coil failed magnetic bearings including large path reluctances is simulated to investigate the effect of path reluctances on imbalance response.**

***Index Terms*—Fault tolerance, magnetic bearings, optimization, path reluctances.**

NOMENCLATURE

A	Pole face area.
b_{sat}	Saturation flux density.
D	Air gap energy matrix.
g_0	Nominal air gap distance.
I	Current vector.
i_b	Bias current.
v_b, v_{cx}, v_{cy}	Bias, x- and y-control voltages.
V_c	Input voltage vector.
K	Current map matrix.
q	Number of active poles.
n	Number of coil turns.
$\hat{R}$	Reluctance matrix.
T	Distribution matrix.
x, y	Rotor displacements.
κ	Power amplifier gain.
σ	Leakage and fringing factor.
ϕ	Magnetic flux.
λ	Lagrange multiplier.
ζ	Sensor sensitivity.
μ_0	Permeability of air.
μ_{rel}	Relative permeability.
θ	Pole face angle.

Manuscript received March 6, 2000; revised July 11, 2000. This work was supported by the Project from NASA Glenn and the Office of Naval Research.

The authors are with the Department of Mechanical Engineering, Texas A&M University, College Station, TX 77843 USA.

Publisher Item Identifier S 0018-9464(00)09962-3.

I. INTRODUCTION

CRITICAL applications of magnetic bearings benefit from a fail-safe control approach. Without this, the many advantages of a magnetic bearing over conventional bearings, such as oil film or rolling element bearings, may be diminished. Fault-tolerant control seeks to provide continued operation of the bearing when power amplifiers or coils suddenly fail. The strong coupling property of a heteropolar magnetic bearing and redefined remaining coil currents make it possible to produce desired force resultants in the x- and y-directions even when some coils fail.

Lyons *et al.* [1], [14] used a three-control axis radial bearing structure with control algorithms for redundant force control and rotor position measurement. Therefore, if one of the coils fails, its control axis can be shut down while maintaining control. A bias current linearization method to accommodate the fault tolerance of magnetic bearings was developed; so the redistribution matrix that linearizes control forces can be obtained even if one or more coils fail [2], [3]. The fault tolerant magnetic bearing system was demonstrated on a large flexible-rotor test rig [4]. Na and Palazzolo [5] developed an optimization method to realize fault-tolerant magnetic bearings; up to five poles failed out of an eight-pole heteropolar magnetic bearing.

Fault-tolerant schemes seek to provide uninterrupted control and high load capacity. Many researchers have investigated the load capacity of a magnetic bearing. Maslen *et al.* [6] presented an expression that describes a maximum bearing load. Bornstein [7] derived equations to express the dynamic load capacity. Rao *et al.* [8] shows that the stiffness capacity of a magnetic bearing can be described as a function of the ratio of dynamic and static loads.

Material path reluctances are usually neglected for the analysis of a small magnetic bearing. However, path reluctances can affect the magnetic forces for a large magnetic bearing or a magnetic bearing with low permeability material. The main contribution of the present work is a determination of the current distribution matrix, which linearizes a fault-tolerant heteropolar magnetic bearing with large material path reluctances, and the resulting load capacity.

II. BEARING MODEL

The magnetic and electric fields of a magnetic bearing can be generally described by using Maxwell's equations. Some discrepancies exist between Maxwell's equations and a one-dimensional magnetic circuit, mainly due to flux leakage,

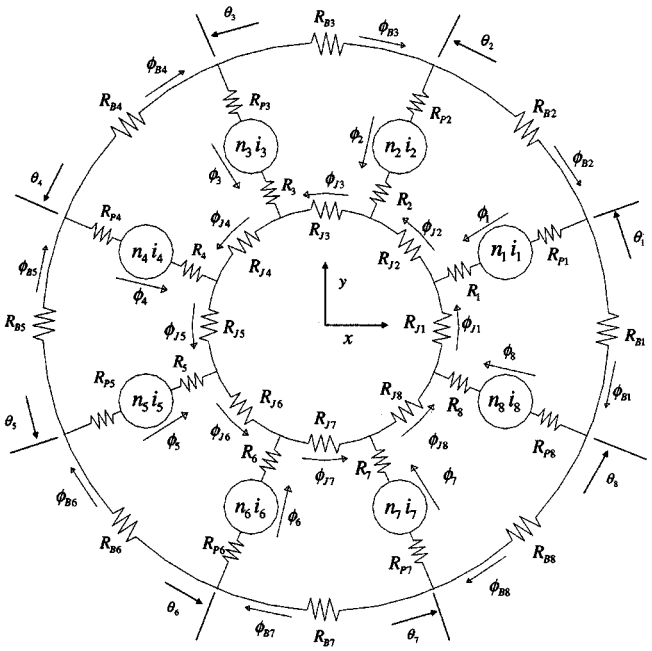

Fig. 1. Eight-pole heteropolar equivalent magnetic circuit.

fringing, and eddy current effects. Finite material path permeability may be included in the magnetic force equations to better predict the current-force relation [9], [10]. Fig. 1 shows the equivalent magnetic circuit of an eight-pole heteropolar magnetic bearing, including material path reluctances.

Material path reluctances for back iron, pole leg, and journal iron segments are described as

$$R_i = \frac{l_i}{\mu_{rel}\mu_0 A_i}, \qquad i = P,\, B,\, J \tag{1}$$

where the areas of the poles, the back iron, and the journal iron are expressed in terms of the pole face area, such as $A_P = \rho_P A$, $A_B = \rho_B A$, and $A_J = \rho_J A$. The length of the pole legs and the length of the back iron and the journal iron between the two poles in terms of the nominal gap distance are $l_P = kg_0$, $l_B = kk_B g_0$, and $l_J = kk_J g_0$. The reluctances in the air gap are described as

$$R_j = \frac{g_0 \hat{g}_j}{\mu_0 A}. \tag{2}$$

The nondimensional air gap equations are

$$\hat{g}_j = 1 - \hat{x}\cos\theta_j - \hat{y}\sin\theta_j \tag{3}$$

where the rotor displacements in nondimensional form are $\hat{x} = x/g_0$ and $\hat{y} = y/g_0$. Apply Ampere's loop law, Gauss's law, and the conservation law of fluxes of the magnetic circuit to obtain a matrix relation

$$\frac{g_0}{\mu_0 A}\hat{R}\Phi = n\hat{N}I. \tag{4}$$

The reluctances in the magnetic bearing can be partitioned into the gap reluctance matrix and the material path reluctance matrix

$$\hat{R} = \Re_g + \Re_m. \tag{5}$$

The gap reluctance matrix is

$$\Re_g = \begin{bmatrix} \hat{g}_1 & -\hat{g}_2 & 0 & 0 & 0 & 0 & 0 & 0 \\ 0 & \hat{g}_2 & -\hat{g}_3 & 0 & 0 & 0 & 0 & 0 \\ 0 & 0 & \hat{g}_3 & -\hat{g}_4 & 0 & 0 & 0 & 0 \\ 0 & 0 & 0 & \hat{g}_4 & -\hat{g}_5 & 0 & 0 & 0 \\ 0 & 0 & 0 & 0 & \hat{g}_5 & -\hat{g}_6 & 0 & 0 \\ 0 & 0 & 0 & 0 & 0 & \hat{g}_6 & -\hat{g}_7 & 0 \\ 0 & 0 & 0 & 0 & 0 & 0 & \hat{g}_7 & -\hat{g}_8 \\ 1 & 1 & 1 & 1 & 1 & 1 & 1 & 1 \end{bmatrix}. \tag{6}$$

The material path reluctance matrix is defined as

$$\Re_m = \alpha\Re_p \tag{7}$$

where, as shown in the equation at the bottom of the next page. The coil turn matrix is

$$\hat{N} = \begin{bmatrix} 1 & -1 & 0 & \cdot & \cdot & 0 \\ 0 & 1 & -1 & 0 & \cdot & \cdot \\ 0 & 0 & 1 & -1 & 0 & \cdot \\ \cdot & \cdot & \cdot & \cdot & \cdot & 0 \\ 0 & \cdot & \cdot & 0 & 1 & -1 \\ 0 & 0 & \cdot & \cdot & 0 & 0 \end{bmatrix}. \tag{8}$$

The magnetic flux vector is then described as

$$\Phi = \frac{\mu_0 An}{g_0}\hat{R}^{-1}\hat{N}I. \tag{9}$$

The flux density in the air gap may be substantially reduced due to the leakage and fringing effects. Allaire [11] showed that the flux leakage and fringing effects in a thrust magnetic bearing can be approximated by a simple scaling factor. The flux density vector in the air gap can be scaled by the leakage and fringing factor σ

$$B = \frac{\sigma\mu_0 n}{g_0}\hat{V}I \tag{10}$$

where

$$\hat{V} = \hat{R}^{-1}\hat{N}.$$

The magnetic forces along the φ direction is given as

$$F_\varphi = -B^T\frac{\partial D}{\partial\varphi}B \tag{11}$$

where $D = g_0 A\hat{D}/(2\mu_0)$ and $\hat{D} = \mathrm{diag}(\hat{g}_j)$. φ is either x or y. The current-force relation, including material path reluctances and leakage and fringing effects, is then described as

$$F_\varphi = -\frac{\sigma^2\mu_0 An^2}{2g_0^2}I^T Q I \tag{12}$$

where

$$Q = \hat{V}^T\frac{\partial\hat{D}}{\partial\hat{\varphi}}\hat{V}.$$

The empirically determined value of σ for a typical homopolar magnetic bearing ranges from 0.8 to 0.9. The currents

distributed to the bearing are related to the control voltage vector with the distribution matrix T [2], [5].

$$I = \kappa T V_c \tag{13}$$

where

$$T = \lfloor T_b T_x T_y \rfloor, \quad V_c = [v_b, v_{cx}, v_{cy}]^T.$$

The bias flux density should be set equal to $b_{\text{sat}}/2$ to obtain maximum magnetic forces at the point of magnetic material saturation. The bias voltage for obtaining the maximum magnetic force is then set as

$$v_b = \frac{g_0 b_{\text{sat}}}{2\kappa\mu_0 n \left|\hat{V} T_b\right|_\infty}. \tag{14}$$

Magnetic force along the φ-direction with the selected v_b and a nondimensional parameter h_φ is

$$F_\varphi = \frac{\sigma^2\kappa^2\mu_0 A n^2 v_b^2}{2g_0^2}\, h_\varphi \tag{15}$$

where

$$h_\varphi = -\hat{V}_c^T T^T \hat{V}^T \frac{\partial \hat{D}}{\partial \hat{\varphi}} \hat{V} T \hat{V}_c,$$
$$\hat{V}_c = \left[1, \frac{v_{cx}}{v_b}, \frac{v_{cy}}{v_b}\right]^T.$$

The magnetic force along the φ-direction becomes a maximum when $v_{c\varphi}$ is equal to v_b. Two examples of distribution matrices for an unfailed eight-pole heteropolar magnetic bearing are

$$T_1 = \begin{bmatrix} 1 & \cos\left(\frac{\pi}{8}\right) & \sin\left(\frac{\pi}{8}\right) \\ -1 & -\cos\left(\frac{3\pi}{8}\right) & -\sin\left(\frac{3\pi}{8}\right) \\ 1 & \cos\left(\frac{5\pi}{8}\right) & \sin\left(\frac{5\pi}{8}\right) \\ -1 & -\cos\left(\frac{7\pi}{8}\right) & -\sin\left(\frac{7\pi}{8}\right) \\ 1 & \cos\left(\frac{9\pi}{8}\right) & \sin\left(\frac{9\pi}{8}\right) \\ -1 & -\cos\left(\frac{11\pi}{8}\right) & -\sin\left(\frac{11\pi}{8}\right) \\ 1 & \cos\left(\frac{13\pi}{8}\right) & \sin\left(\frac{13\pi}{8}\right) \\ -1 & -\cos\left(\frac{15\pi}{8}\right) & -\sin\left(\frac{15\pi}{8}\right) \end{bmatrix}$$

$$T_2 = \begin{bmatrix} 1 & 1 & 0 \\ -1 & 0 & -1 \\ 1 & 0 & 1 \\ -1 & 1 & 0 \\ 1 & -1 & 0 \\ -1 & 0 & 1 \\ 1 & 0 & -1 \\ -1 & -1 & 0 \end{bmatrix}.$$

Eight independent currents are distributed to the bearing via the distribution matrix of T_1, whereas four independent currents are distributed via T_2. The row number for these matrices corresponds to the pole number in Fig. 1. The typical distribution matrix used in a C core heteropolar magnetic bearing control

---

$$\alpha = \frac{k}{\mu_{re\ell}\rho_P}$$

$$\Re_p = \begin{bmatrix} 1+\frac{\eta}{8} & -1-\frac{6\eta}{8} & -\frac{5\eta}{8} & -\frac{4\eta}{8} & -\frac{3\eta}{8} & -\frac{2\eta}{8} & -\frac{\eta}{8} & 0 \\ \frac{\eta}{8} & 1+\frac{2\eta}{8} & -1-\frac{5\eta}{8} & -\frac{4\eta}{8} & -\frac{3\eta}{8} & -\frac{2\eta}{8} & -\frac{\eta}{8} & 0 \\ \frac{\eta}{8} & \frac{2\eta}{8} & 1+\frac{3\eta}{8} & -1-\frac{4\eta}{8} & -\frac{3\eta}{8} & -\frac{2\eta}{8} & -\frac{\eta}{8} & 0 \\ \frac{\eta}{8} & \frac{2\eta}{8} & \frac{3\eta}{8} & 1+\frac{4\eta}{8} & -1-\frac{3\eta}{8} & -\frac{2\eta}{8} & -\frac{\eta}{8} & 0 \\ \frac{\eta}{8} & \frac{2\eta}{8} & \frac{3\eta}{8} & \frac{4\eta}{8} & 1+\frac{5\eta}{8} & -1-\frac{2\eta}{8} & -\frac{\eta}{8} & 0 \\ \frac{\eta}{8} & \frac{2\eta}{8} & \frac{3\eta}{8} & \frac{4\eta}{8} & \frac{5\eta}{8} & 1+\frac{6\eta}{8} & -1-\frac{\eta}{8} & 0 \\ \frac{\eta}{8} & \frac{2\eta}{8} & \frac{3\eta}{8} & \frac{4\eta}{8} & \frac{5\eta}{8} & \frac{6\eta}{8} & 1+\frac{7\eta}{8} & -1 \\ 0 & 0 & 0 & 0 & 0 & 0 & 0 & 0 \end{bmatrix}$$

$$\eta = \frac{\rho_P(\rho_J k_B + \rho_B k_J)}{\rho_B \rho_J}$$

is T_2. Only two controller outputs are needed for the distribution matrix of T_2, whereas eight independent controller outputs are needed for the distribution matrix of T_1. The magnetic force generated by currents distributed with T_1 or T_2 is completely decoupled. The control voltage of v_{cy} does not affect the magnetic force along the x-direction. The parameter h_φ with the distribution matrix of T_1 in case of no path reluctances at the bearing center position ($x = y = 0$) and $v_{c\varphi} = v_b$ is equal to eight. Thus, the maximum magnetic force of the eight-pole heteropolar bearing calculated with no material path reluctances is simplified as

$$F_x^{\max} = F_y^{\max} = \frac{4\sigma^2\mu_0 An^2 i_b^2}{g_0^2}, \tag{16}$$

where $i_b = \kappa v_b$. A distribution matrix for the four-pole heteropolar magnetic bearing is

$$T = \begin{bmatrix} 1 & 1 & 0 \\ -1 & 0 & -1 \\ 1 & -1 & 0 \\ -1 & 0 & 1 \end{bmatrix}.$$

Similarly, the maximum magnetic force of the four-pole heteropolar bearing without path reluctance is calculated as

$$F_x^{\max} = F_y^{\max} = \frac{2\sigma^2\mu_0 An^2 i_b^2}{g_0^2}. \tag{17}$$

The eight-pole heteropolar magnetic bearing used in this analysis has g_0(0.000 508 m), A(0.000 602 m^2), l_P(0.03 m), l_B(0.065 m), l_J(0.021 m), n(50), ρ_P(0.985), ρ_B(0.98), and ρ_J(0.985). The parameters b_{sat}, σ, and κ are assumed to be 1.2 Tesla, 0.85, and 1, respectively. The maximum magnetic forces and corresponding bias voltages and h_φ with T_1 and T_2 with respect to α are shown in Fig. 2.

The maximum force does not decrease much as α is increased; however, the bias voltage needed for the maximum force increases rapidly. Therefore, saturation of magnetic bearing will occur at a higher current $i_{\text{sat}} = 2i_b$ as α is increased. The maximum magnetic force calculated with T_2 is just 92% of the maximum magnetic force calculated with T_1, whereas the same current inputs are required. This shows that the control with eight independent control currents maximizes the magnetic force with lower risk of flux saturation.

III. Linearized Forces

Linearized forces can be determined for a heteropolar magnetic bearing, including path reluctances. Nonlinear magnetic forces are defined as

$$F_\varphi = I^T \frac{\partial U}{\partial \varphi} I \tag{18}$$

where

$$U = \frac{\sigma^2\mu_0 An^2}{2g_0} \hat{V}^T \hat{D} \hat{V}.$$

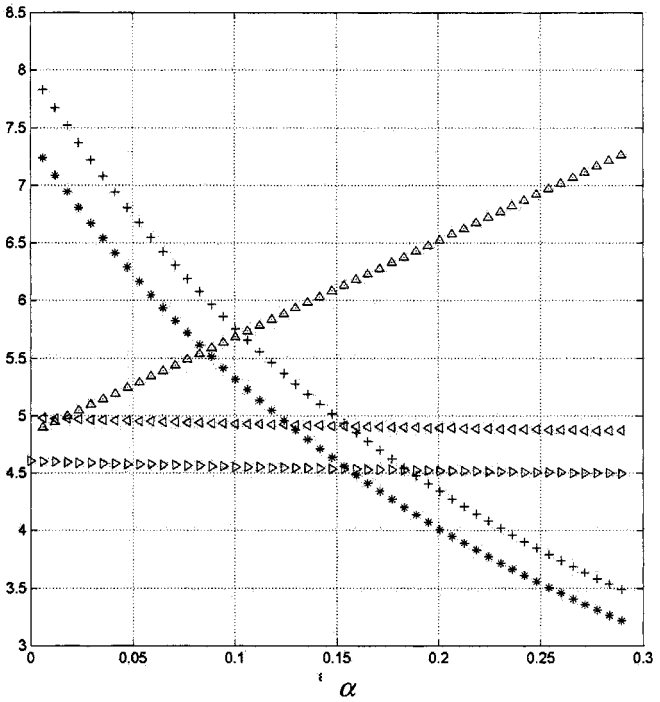

Fig. 2. Maximum force, bias voltage, and h_φ versus α: $\triangleleft: F_\varphi^{\max}(T_1)/100$, $\triangleright: F_\varphi^{\max}(T_2)/100$, $\triangle: v_b$, $+: h_\varphi(T_1)$, $*: h_\varphi(T_2)$.

Partial differentiations of U can be rewritten as a nondimensional form

$$\frac{\partial U}{\partial \varphi} = \frac{\sigma^2\mu_0 An^2}{2g_0^2} \hat{U}_\varphi \tag{19}$$

where

$$\hat{U}_\varphi = -\hat{V}^T \frac{\partial \hat{D}}{\partial \hat{\varphi}} \hat{V}.$$

Similarly

$$\frac{\partial^2 U}{\partial \varphi \partial \omega} = \frac{\sigma^2\mu_0 An^2}{g_0^3} \hat{U}_{\omega\varphi} \tag{20}$$

where

$$\hat{U}_{\omega\varphi} = -\hat{V} \frac{\partial \hat{D}}{\partial \hat{\omega}} \left(\frac{\partial \hat{V}}{\partial \hat{\varphi}} \right)^T$$

$$\frac{\partial \hat{V}}{\partial \hat{\varphi}} = -\hat{R}^{-1} \frac{\partial \hat{R}}{\partial \hat{\varphi}} \hat{R}^{-1} \hat{N}.$$

φ and ω both represent x- or y-direction. The nonlinear magnetic forces with path reluctances can also be linearized about the bearing center position and the zero control voltages by using Taylor series expansion

$$F_x \approx -K_{pxx}x - K_{pxy}y + K_{vxx}v_{cx} + K_{vxy}V_{cy} \tag{21}$$

$$F_y \approx -K_{pyx}x - K_{pyy}y + K_{vyx}v_{cx} + K_{vyy}v_{cy} \tag{22}$$

where position stiffnesses and voltage stiffnesses are defined as

$$K_{p\omega\varphi} = -\frac{\partial F_\omega}{\partial \varphi} = -\frac{\sigma^2\kappa^2\mu_0 An^2 v_b^2}{g_0^3} T_b^T \hat{U}_{\omega\varphi 0} T_b \tag{23}$$

$$K_{v\omega\varphi} = \frac{\partial F_\omega}{\partial v_{c\varphi}} = \frac{\sigma^2\kappa^2\mu_0 An^2 v_b}{g_0^2} T_b^T \hat{U}_{\omega 0} T_\varphi. \tag{24}$$

The position stiffnesses and voltage stiffnesses are calculated with the distribution matrices of T_1 and T_2 at the center position of the bearing. No cross-coupled position and voltage stiffnesses exist because the distribution matrices T_1 and T_2 completely decouple the magnetic forces. Linearized forces with T_1 and T_2 are then reduced as

$$F_x \approx -K_p x + K_v v_{cx} \tag{25}$$

$$F_y \approx -K_p y + K_v v_{cy}. \tag{26}$$

Fig. 3 shows that K_p and K_v calculated with the distribution matrices T_1 and T_2 are reduced as α is increased. The values of K_p, K_v, and v_b with T_1 at $\alpha = 0$ are $-1\,358\,000$ N/m, 142.2 N/V, and 4.851, respectively.

IV. Determination of the Distribution Matrices

It is shown that large path reluctances in a heteropolar magnetic bearing have a considerable influence on the flux distribution. The coil current distribution of bias currents, x-control currents, and y-control currents must be redefined in the case of single or multiple coil failures to produce the same force resultants. If some coils fail, the reduced current vector is related by defining a matrix K

$$I = K\hat{I} \tag{27}$$

where the reduced current vector is defined as

$$\hat{I} = \hat{T}V_c. \tag{28}$$

The reduced distribution matrix is

$$\hat{T} = \left[\hat{T}_b, \hat{T}_x, \hat{T}_y\right] \tag{29}$$

where

$$\hat{T}_b = [t_1, t_2, \ldots, t_q]^T, \quad \hat{T}_x = [t_{q+1}, t_{q+2}, \ldots, t_{2q}]^T$$
$$\hat{T}_y = [t_{2q+1}, t_{2q+2}, \ldots, t_{3q}]^T.$$

To yield the linearized forces that are described as

$$F_\varphi = v_b v_{c\varphi}. \tag{30}$$

The necessary conditions are [2], [5]

$$\hat{T}^T G_\varphi \hat{T} - M_\varphi = \underline{0}, \tag{31}$$

where

$$G_\varphi = -\frac{\mu_0 A n^2}{2g_0^2} K^T \hat{V}^T \frac{\partial \hat{D}}{\partial \hat{\varphi}} \hat{V} K,$$

$$M_x = \begin{bmatrix} 0 & 0.5 & 0 \\ 0.5 & 0 & 0 \\ 0 & 0 & 0 \end{bmatrix}, \quad M_y = \begin{bmatrix} 0 & 0 & 0.5 \\ 0 & 0 & 0 \\ 0.5 & 0 & 0 \end{bmatrix}.$$

The optimization method for obtaining distribution matrices using Lagrange multipliers can be applied on a heteropolar magnetic bearing, including path reluctances. A cost function is defined in a manner that the Euclidean norm of flux density vector B is weighted with a diagonal matrix P

$$J(\hat{T}) = B(\hat{T})^T P B(\hat{T}). \tag{32}$$

The weighting matrix P can be assigned so that the load capacity in a specific direction is increased. The weighting matrix P is selected as

$$P = \frac{\partial D}{\partial y}. \tag{33}$$

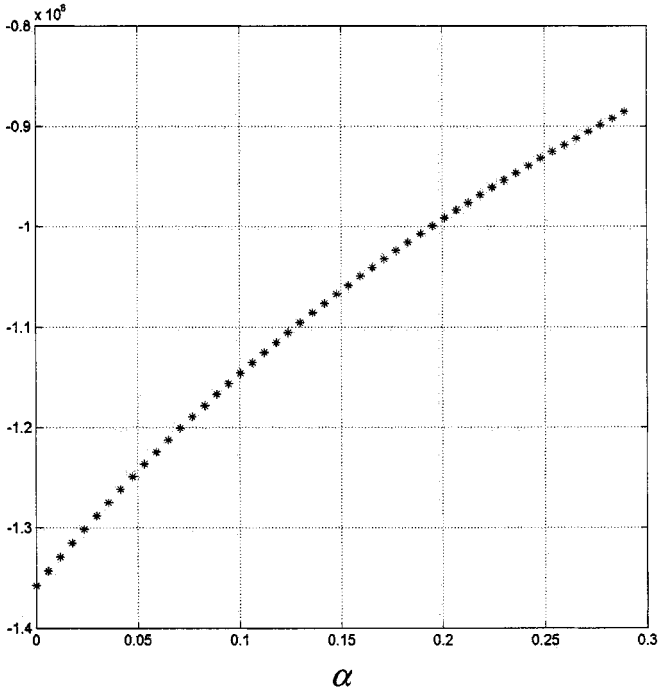

(a)

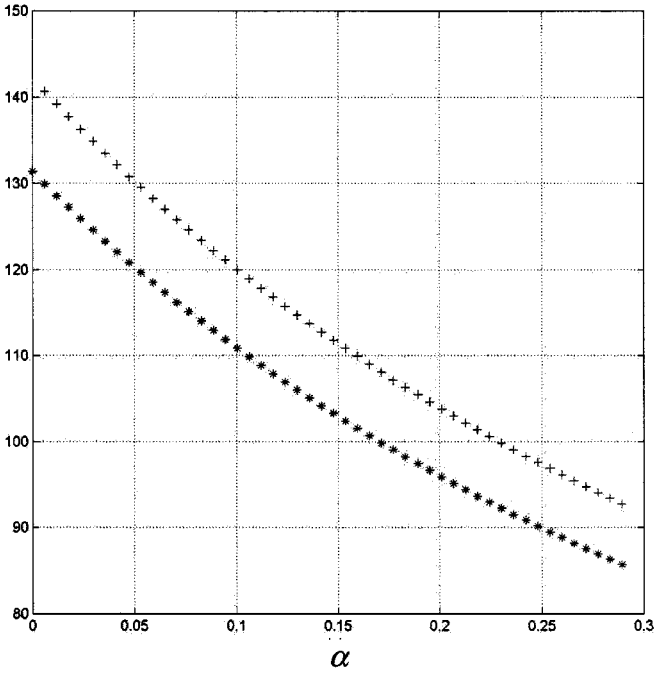

(b)

Fig. 3. (a) Position stiffness (K_p) (same for T_1 and T_2). (b) Voltage stiffness ($+$: $K_v(T_1)$, $*$: $K_v(T_2)$).

The cost function then represents the magnetic force along the y-direction. Twelve equality constraint equations are also derived from (31)

$$h_1(\hat{T}) = \hat{T}_b^T G_x \hat{T}_b = 0,$$
$$h_2(\hat{T}) = \hat{T}_b^T G_x \hat{T}_x - 0.5 = 0,$$
$$h_3(\hat{T}) = \hat{T}_b^T G_x \hat{T}_y = 0,$$
$$h_4(\hat{T}) = \hat{T}_x^T G_x \hat{T}_x = 0,$$
$$h_5(\hat{T}) = \hat{T}_x^T G_x \hat{T}_y = 0,$$

$$
\begin{aligned}
h_6(\hat{T}) &= \hat{T}_y^T G_x \hat{T}_y = 0,\\
h_7(\hat{T}) &= \hat{T}_b^T G_y \hat{T}_b = 0,\\
h_8(\hat{T}) &= \hat{T}_b^T G_y \hat{T}_x = 0,\\
h_9(\hat{T}) &= \hat{T}_b^T G_y \hat{T}_y - 0.5 = 0,\\
h_{10}(\hat{T}) &= \hat{T}_x^T G_y \hat{T}_x = 0,\\
h_{11}(\hat{T}) &= \hat{T}_x^T G_y \hat{T}_y = 0,\\
h_{12}(\hat{T}) &= \hat{T}_y^T G_y \hat{T}_y = 0. \qquad (34)
\end{aligned}
$$

The Lagrange multiplier method can be applied to the basic problem to solve for $\hat{T}$ that satisfies (31). Define

$$\hat{L}(\hat{T}) = B(\hat{T})^T P B(\hat{T})^T + \sum_{j=1}^{12} \lambda_j h_j(\hat{T}). \qquad (35)$$

The partial differentiation of (35) with respect to t_i and λ_j leads to $3q+12$ nonlinear algebraic equations to solve for t_i and λ_j

$$w_i = \frac{\partial \hat{L}}{\partial t_i} = 0, \qquad i = 1, 2, \ldots, 3q, \qquad (36)$$

$$w_{(j+3q)} = h_j(\hat{T}) = 0, \qquad j = 1, 2, \ldots, 12. \qquad (37)$$

A vector form of $3q+12$ nonlinear algebraic equations is

$$W(t, \lambda) = \begin{bmatrix} w_1(t, \lambda) \\ w_2(t, \lambda) \\ \cdot \\ \cdot \\ \cdot \\ w_{(3q+11)}(t, \lambda) \\ w_{(3q+12)}(t, \lambda) \end{bmatrix} = \begin{bmatrix} 0 \\ 0 \\ \cdot \\ \cdot \\ \cdot \\ 0 \\ 0 \end{bmatrix}. \qquad (38)$$

V. Optimal Solutions for the Distribution Matrices

Distribution matrices for a heteropolar magnetic bearing, including path reluctances, are obtained by solving the system of nonlinear algebraic equations shown in (38). A least-squares iterative method (MATLAB) was used to solve the system of nonlinear algebraic equations, which yields multiple solutions. Various initial guesses of t_i and λ_j may be tested to obtain converged solutions. The parameter μ_{rel} equals 500 for calculation of the distribution matrices. The distribution matrices for 1–3rd coils failed, 1–2–3rd coils failed, 5th–8th coils failed, and 2–4–6–7–8th coils failed magnetic bearings are calculated as

$$T_{13} = \begin{bmatrix} 0 & 0 & 0 \\ 0.38794 & 0.13363 & 0.40059 \\ 0 & 0 & 0 \\ 0.41082 & -0.26587 & 0.37758 \\ -0.06265 & 0.26700 & 0.41101 \\ 0.08070 & 0.18900 & 0.29271 \\ 0.48197 & 0.15528 & -0.15589 \\ 0.47281 & 0.52258 & -0.01879 \end{bmatrix},$$

$$T_{123} = \begin{bmatrix} 0 & 0 & 0 \\ 0 & 0 & 0 \\ 0 & 0 & 0 \\ 1.579990 & -0.0176 & 0.1711 \\ 0.612027 & 0.2123 & 0.2221 \\ 0.495525 & 0.1632 & 0.1814 \\ 1.799341 & 0.1880 & 0.0165 \\ 1.145192 & 0.2137 & 0.1547 \end{bmatrix},$$

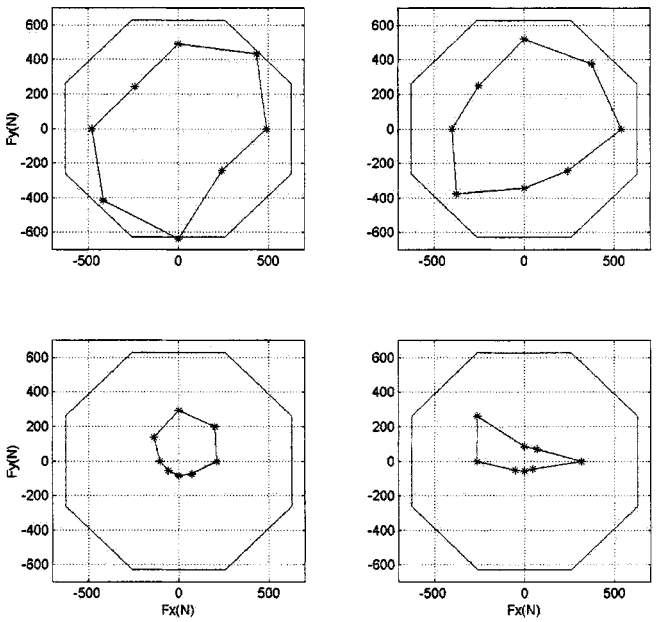

Fig. 4. Load capacity of the fault-tolerant magnetic bearing with path reluctances for 1–3rd coils failed (upper left), 1–2–3rd coils failed (upper right), 5–6–7–8th coils failed (bottom left), and 2–4–6–7–8th coils failed (bottom right).

$$T_{5678} = \begin{bmatrix} 2.94444 & 0.0770 & -1.2560 \\ 1.83753 & -0.1083 & -1.3101 \\ 1.83754 & 0.1083 & -1.3101 \\ 2.94444 & -0.0770 & -1.2560 \\ 0 & 0 & 0 \\ 0 & 0 & 0 \\ 0 & 0 & 0 \\ 0 & 0 & 0 \end{bmatrix},$$

$$T_{24\,678} = \begin{bmatrix} 8.06183 & 0.0775 & -0.2336 \\ 0 & 0 & 0 \\ 3.71891 & -0.0363 & 0.0418 \\ 0 & 0 & 0 \\ 8.06183 & 0.0402 & -0.2491 \\ 0 & 0 & 0 \\ 0 & 0 & 0 \\ 0 & 0 & 0 \end{bmatrix}.$$

The solutions for a multiple-coils-failed bearing are well converged; so the solutions satisfy (31) with tolerable errors. For example, T_{5678} satisfies (31) with minimal error, such as

$$\hat{T}^T G_x \hat{T} = \begin{bmatrix} 0 & 0.5 & 0 \\ 0.5 & 0 & -0.00025 \\ 0 & -0.00025 & 0 \end{bmatrix},$$

$$\hat{T}^T G_y \hat{T} = \begin{bmatrix} 0 & 0 & 0.5 \\ 0 & 0.00017 & 0 \\ 0.5 & 0 & 0.00013 \end{bmatrix}.$$

The load capacities of a heteropolar magnetic bearing including path reluctances with multiple poles failed, are calculated for the calculated distribution matrices of T_{13}, T_{123}, T_{5678}, and $T_{24\,678}$ and shown in Fig. 4.

The outer locus shows the unfailed bearing load capacity, whereas the inner locus shows the failed bearing load capacities for eight directions. The position stiffnesses and voltage

TABLE I

	T_{13}	T_{123}	T_{5678}	T_{24678}
v_b	19.53	4.43	5	1.09
K_{pxx} (N/m)	-787681	-439170	-1221422	-580702
K_{pxy} (N/m)	180972	197822	-0.09	-183119
K_{pyx} (N/m)	180972	197822	-0.09	-183119
K_{pyy} (N/m)	-668967	-431316	-46624	-214463
K_{vxx} (N/Volt)	19.53	4.43	5	1.09
K_{vxy} (N/Volt)	0	0	0	0
K_{vyx} (N/Volt)	0	0	0	0
K_{vyy} (N/Volt)	19.53	4.43	5	1.09

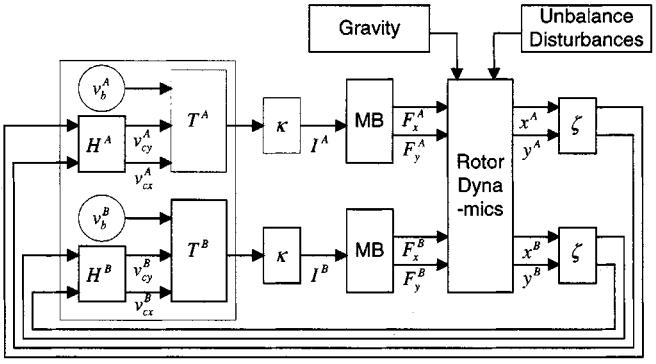

Fig. 5. Schematic of control system.

stiffnesses for the distribution matrices of T_{13}, T_{123}, T_{5678}, and $T_{24\,678}$ are also calculated at the center position of the bearing. The voltage stiffnesses are completely decoupled for valid T. However, some cross-coupled position stiffnesses for failed bearings exist due to unevenly distributed flux densities. The calculated position stiffness and voltage stiffness and bias voltage gain are shown in Table I. The voltage stiffnesses K_{vxx} and K_{vyy} for a valid T should be equal to the bias voltage v_b because the distribution matrix T is calculated for the linearized forces shown in (30).

VI. Control System Design and Simulations

A fault-tolerant control system of a horizontal rigid rotor supported on magnetic bearings is constructed. The schematic of the fault-tolerant control system is shown in Fig. 5. A symmetric, horizontal rigid rotor has mass of 10.7 kg, polar moment of inertia of 0.008 kgm^2, transverse moment of inertia about the mass centor of 0.36 kgm^2, and bearing locations of 0.22 m on each side of the mass center. Unbalances of eccentricity of 2.5 E-6 are applied on two bearing locations with a relative phase angle 90°.

The sensor sensitivity ζ is 7874 V/m. The power amplifier gain κ is 1 A/V. The control law was designed with simple PD control and low-pass filters. The closed loop bearing stiffness and damping can be adjusted by tuning the PD controller gains, k_p and k_d [12]. Rotor critical speeds and their corresponding dampings can be designed by tuning active bearing properties [13].

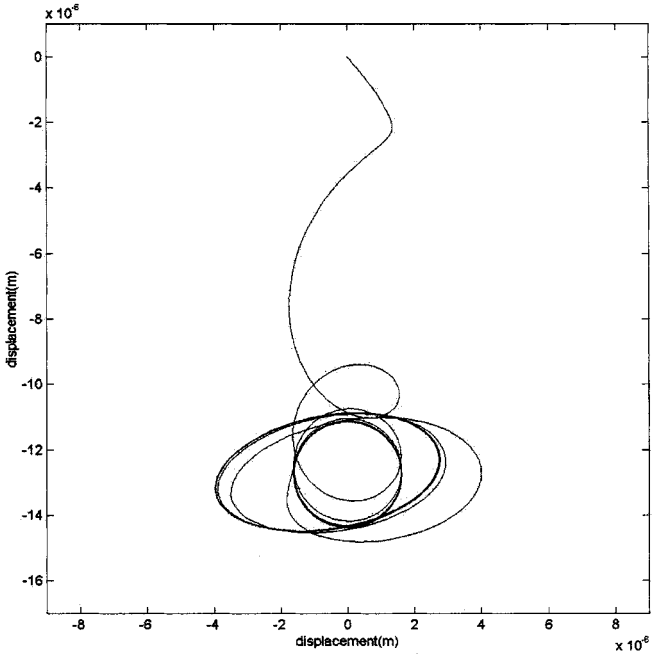

Fig. 6. Orbit plot for normal operation to the 5–6–7–8th poles failed operation.

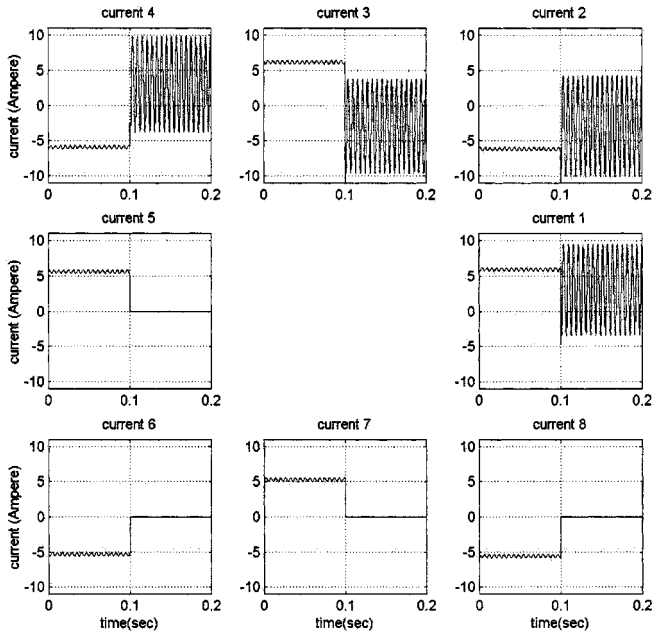

Fig. 7. Current inputs for normal operation to the 5–6–7–8th poles failed operation.

The following system dynamics simulation illustrates the transient response of a rotor supported by magnetic bearings during a coil failure event. A distribution matrix of T_1 is used to distribute currents to the unfailed bearings. The parameters K_p, K_v, and v_b with T_1 at $\alpha = 0.1181$ ($\mu_{\rm rel} = 500$) for unfailed bearings are $-1\,152\,000$ N/m, 116.78 N/V, and 5.836, respectively. The designed PD control gains k_p and k_d for the unfailed bearings are -4.6 and -0.02, respectively. A new distribution matrix and control gains should be provided to produce desired force resultants when some coils in a magnetic

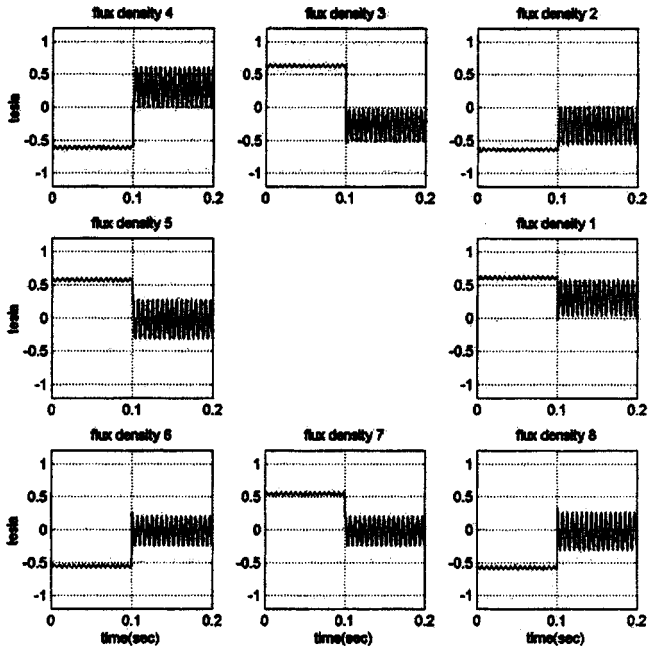

Fig. 8. Flux densities for normal operation to the 5–6–7–8th poles failed operation.

bearing fail suddenly. The transient response from normal operation to fault-tolerant control with 5–6–7–8th coils failed for both bearings was simulated for nonlinear bearings with path reluctances at 10 000 RPM. The distribution matrix of T_1 was switched to T_{5678} when four adjacent coils failed at 0.1 second. The PD control gains k_p and k_d for the failed bearings were adjusted as -92 and -0.35, respectively. Transient response of the orbit at bearing A is shown in Fig. 6. The orbit after failure becomes elliptic due to asymmetric position stiffnesses of the failed bearings. Transient response of the current inputs to bearing A for the 5–6–7–8th poles failed case is shown in Fig. 7. This shows that large currents are required to maintain similar dynamic properties before and after failure. Transient response of the flux densities in Bearing A is shown in Fig. 8. The adjusted distribution matrix of T_{5678} yields the required inactive pole fluxes so that the bearing has the necessary forces to maintain stability. The load capacity is considerably reduced, though, in the failed bearing.

VII. Conclusion

Material path reluctances are usually neglected for the calculation of fluxes and magnetic forces; however, they may significantly influence fluxes and magnetic forces for a large magnetic bearing or a magnetic bearing with low relative permeability. Therefore, material path reluctances should be included in the calculation of distribution matrices for fault-tolerant control. The control with eight independent control currents maximizes the magnetic force but requires more controller outputs. A Lagrange multiplier optimization method is used to determine distribution matrices for the magnetic bearing, including large path reluctances. The distribution matrices are calculated up to a certain combination of five poles failed out of eight poles. Nondimensional forms of the position stiffnesses and voltage stiffnesses are calculated for the fault-tolerant magnetic bearings. Simulations show that distribution matrices calculated for a magnetic bearing with large material reluctances can still provide good control.

Acknowledgment

The authors would like to thank A. Kascak, G. Montague, R. Jansen, A. Provenza, T. Calvert, L. Peterson and G. Bell for technical support.

References

[1] J. P. Lyons, M. A. Preston, R. Gurumoorthy, and P. M. Szczesny, "Design and control of a fault-tolerant active magnetic bearing system for aircraft engine," in *Proc. 4th Int. Symp. Magnetic Bearings*, ETH Zurich, 1994, pp. 449–454.

[2] E. H. Maslen and D. C. Meeker, "Fault tolerance of magnetic bearings by generalized bias current linearization," *IEEE Trans. Magn.*, vol. 31, pp. 2304–2314, 1995.

[3] D. C. Meeker, "Optimal solutions to the inverse problem in quadratic magnetic actuators," Ph.D. dissertation, Univ. Virginia, 1996.

[4] E. H. Maslen, C. K. Sortore, G. T. Gillies, R. D. Williams, S. J. Fedigan, and R. J. Aimone, "Fault tolerant magnetic bearings," *J. Eng. Gas Turbines Power*, vol. 121, pp. 504–508, 1999.

[5] U. J. Na and A. B. Palazzolo, "Optimized realization of fault-tolerant heteropolar magnetic bearings for active vibration control," in *Proc. 1999 ASME Design Eng. Tech. Conf.*, Las Vegas, NV, Sept. 12–15, 1999, Paper VIB-8258.

[6] E. H. Maslen, P. Hermann, M. Scott, and R. R. Humphris, "Practical limits to the performance of magnetic bearings: Peak force, slew rate, and displacement sensitivity," *J. Tribol.*, vol. 111, pp. 331–336, 1989.

[7] K. R. Bornstein, "Dynamic load capabilities of active electromagnetic bearings," *J. Tribol.*, vol. 113, pp. 598–603, 1991.

[8] D. K. Rao, G. V. Brown, P. Lewis, and J. Hurley, "Stiffness of magnetic bearings subjected to combined static and dynamic loads," *J. Tribol.*, vol. 114, pp. 785–789, 1992.

[9] J. D. Knight, Z. Xia, E. McCaul, and H. Hacker Jr., "Determination of forces in a magnetic bearing actuator: Numerical computation with comparison to experiment," *J. Tribol.*, vol. 114, pp. 796–801, 1992.

[10] P. E. Allaire, R. L. Fittro, E. H. Maslen, and W. C. Wakefield, "Measured force/current relations in solid magnetic thrust bearings," *J. Eng. Gas Turbines Power*, vol. 119, pp. 131–142, 1997.

[11] P. E. Allaire, "Design and test of a magnetic thrust bearing," *J. Franklin Inst.*, vol. 326, pp. 831–847, 1989.

[12] F. J. Keith, R. D. Williams, and P. E. Allaire, "Digital control of magnetic bearings supporting a multimass flexible rotor," *STLE Tribol. Trans.*, vol. 33, pp. 307–314, 1990.

[13] J. M. Vance, *Rotordynamics of Turbomachinery*. New York: Wiley, 1988.

[14] J. C. Maxwell, *A Treatise on Electricity and Magnetism*, 3rd ed. Oxford: Clarendon, 1892, vol. 2, pp. 68–73.